Wei, W., et al., 2022, Boron proxies record paleosalinity variation in the North American Midcontinent Sea in response to Carboniferous glacio-eustasy: Geology, https://doi.org/10.1130/G49521.1

SUPPLEMENTAL ONLINE MATERIAL

Boron proxies record paleosalinity variation in the North American Midcontinent Sea in response to Carboniferous glacio-eustasy

Wei Wei, Wenchao Yu, Thomas J. Algeo, Achim D. Herrmann, Lian Zhou, Jinhua Liu, Qian Wang, Yuansheng Du

AUXILIARY FIGURES

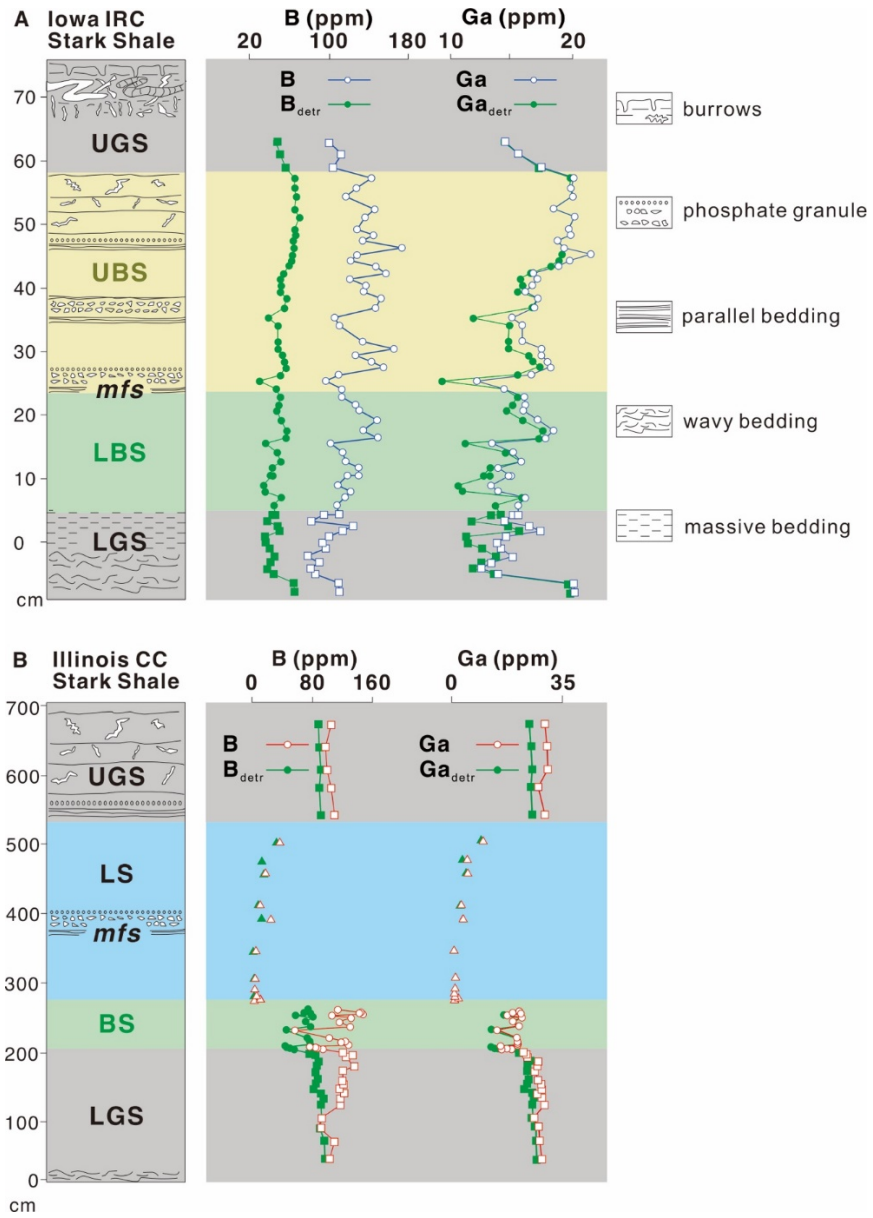

Figure S1. B and Ga concentrations of Stark Shale from (A) IRC and (B) CC. BS = black shale (circles), GS = gray shale (squares), LS = limestone (triangles; $CaCO_3$ >40%), and "L" and "U" prefixes for BS and GS indicate "lower" and "upper", respectively. *mfs* = maximum flooding surface; detr = detrital. Note that the difference between the total concentration and the detrital fraction (for either B or Ga) represents the seawater-sourced (hydrogenous) fraction. For calculation of detrital B and Ga concentrations, see below.

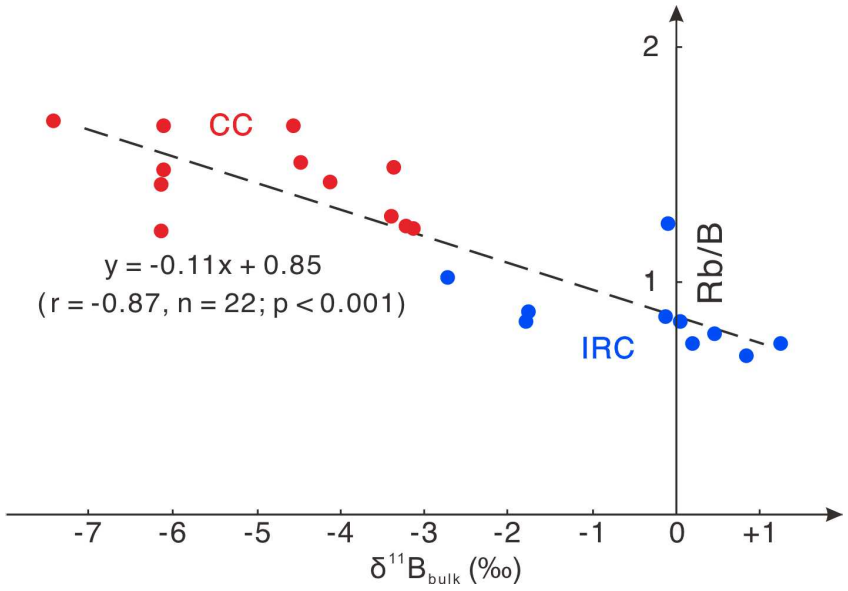

Figure S2. Crossplot of Rb/B versus $\delta^{11}B$ for shale samples from IRC (blue) and CC (red), showing strong negative covariation ($r = –0.87$; $p < 0.001$). This relationship reflects mixing of Rb-rich illite (deposited more proximally) and Rb-poor smectite (deposited more distally) and is similar to that reported for modern marine shales (Ishikawa and Nakamura, 1993). B in the illitic component is mostly detrital in origin and exhibits $\delta^{11}B$ closer to the detrital value (–9.1‰), whereas a large fraction of B in the smectitic component is in the form of $B(OH)_4^-$ adsorbed from seawater (~+19‰ to +24‰), yielding higher bulk-shale $\delta^{11}B$. This relationship supports interpretation of bulk-shale $\delta^{11}B$ as an effective paleosalinity proxy.

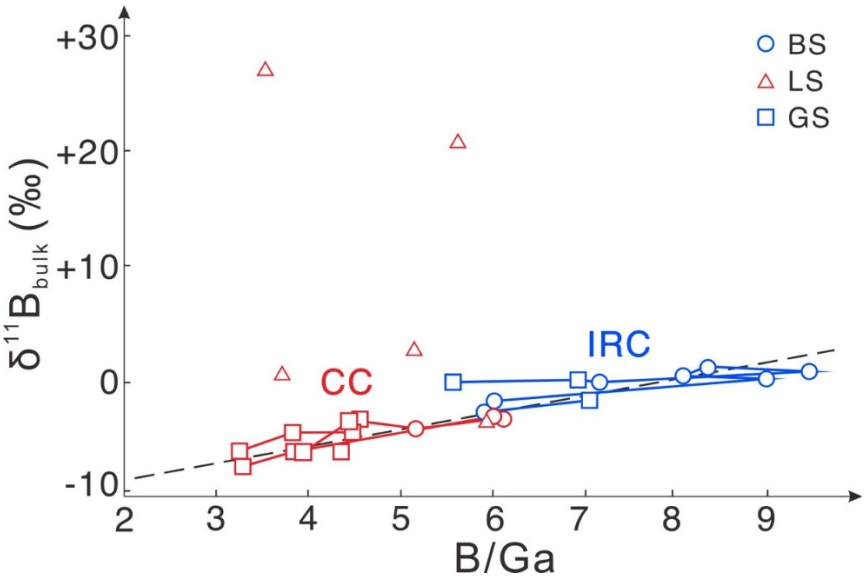

Figure S3. Crossplot of $\delta^{11}B$ versus B/Ga for both shale and limestone samples from IRC (blue) and CC (red). The few limestone samples (LS, triangles; $n = 5$) analyzed in this study yield higher $\delta^{11}B$ (to +27‰) and are non-colinear with the black shales (BS, circle) and gray shales (GS, squares) [note: shale data and dashed regression line are the same as those in Figure 3 of the main text]. Note that B/Ga values at CC are similar for both shale and limestone samples, suggesting that the B/Ga of both lithologies is a robust paleosalinity proxy; differences in their $\delta^{11}B$ values may reflect lithology-dependent B species uptake or the lack of detrital B in the limestone samples.

ROLE OF NORMALIZATION OF BORON TO GALLIUM

The reason for using an elemental ratio (i.e., B/Ga) rather than a simple concentration (i.e., [B]) to evaluate paleosalinity is that concentrations are highly susceptible to lithologic influences—for example, [B] is typically 15-20 ppm in shales but <1 ppm in limestones, so [B] variation will be heavily influenced by lithology in mixed limestone-shale successions. The elements B, Al, and Ga all belong to Group 13 ("boron group") of the periodic table. The advantages of Ga rather than Al as a normalizer for B are that, compared to Al, the concentration of Ga in the sediment is much closer to that of B, and its behavior in aqueous systems is opposite that of B (i.e., Ga concentrations are higher in freshwater systems), enhancing the effectiveness of B/Ga as a paleosalinity proxy (Wei and Algeo, 2020).

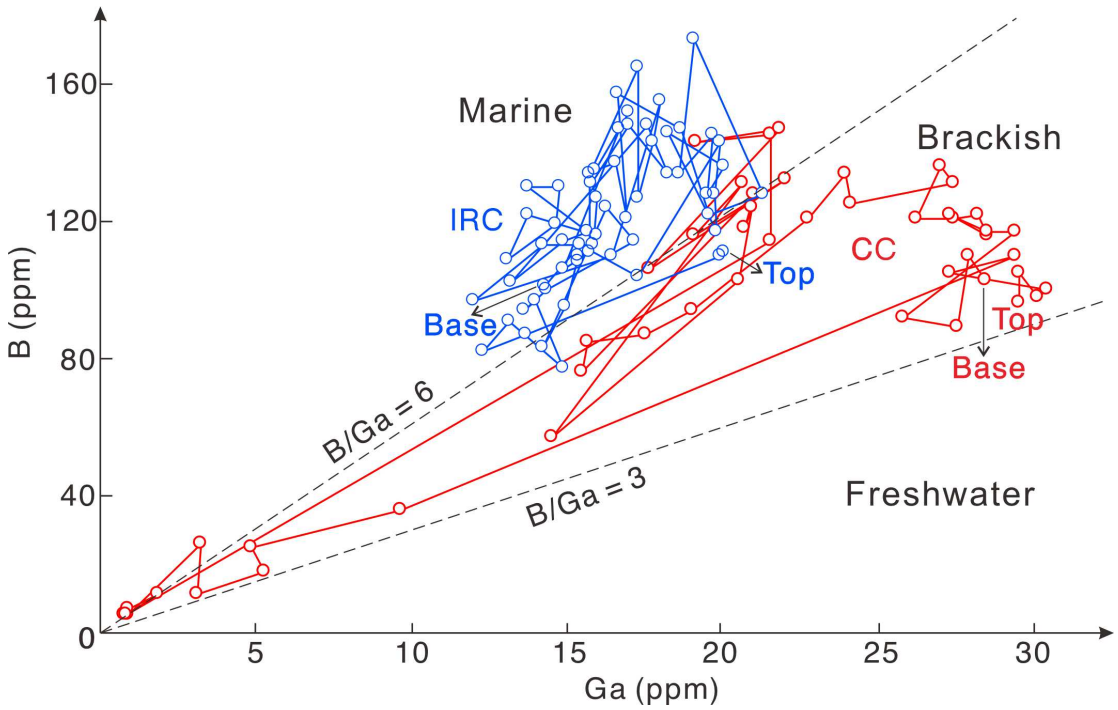

Figure S4. Covariation of B versus Ga for the IRC (blue) and CC (red) study cores. Both sections exhibit strong positive covariation: IRC (r = +0.59, p < 0.01) and CC (r = +0.87, p < 0.01), reflecting lithologic influence on raw [B] and [Ga] concentrations. The solid lines connect samples in stratigraphic order from the base to the top of each study core. The dashed lines represent salinity facies thresholds between marine (B/Ga > 6), brackish (3-6), and freshwater (< 3) samples (from Wei and Algeo, 2020). Higher B/Ga ratios signify higher salinities at IRC (mostly marine) relative to CC (mostly brackish), recording a pronounced lateral gradient in salinity across the NAMS from the Midcontinent Shelf (marine) to the Illinois Basin (brackish).

CALCULATION OF SEAWATER-SOURCED BORON FRACTION

In siliciclastic formations containing a significant clay mineral fraction, crossplots of Al versus B and Al versus Ga allow estimation of the abundances of the detrital and hydrogenous fractions of each element for each sample (Fig. S5). For Ga, strong positive covariation with Al demonstrates that most Ga is resident in the detrital fraction (Spivack et al., 1987; Wei and Algeo, 2020), yielding similar estimates of detrital Ga/Al (2.7 ppm/%) for both IRC and CC.

For B, a ratio fitting the base of the data field at CC provides the best estimate of detrital B/Al (9±1 ppm/%), and the same value was applied to IRC. For all plots, excess B and Ga above the dashed detrital lines represent the seawater-sourced (hydrogenous) fractions of each element. Computationally, $B_{detr} = (B/Al)_{detr} \times Al$, and $B_{sw} = B_{total} - B_{detr}$.

The isotopic composition of B_{sw} was calculated as $\delta^{11}B_{sw} = (\frac{\delta^{11}B_{meas} \times B_{total} - \delta^{11}B_{detr} \times B_{detr}}{B_{sw}})$, where $\delta^{11}B_{meas}$ is the measured composition of bulk boron, and $\delta^{11}B_{detr}$ was assumed to be –9.1±2.4‰ based on the B-isotopic composition of average continental crust (Lemarchand et al., 2012; Gaillardet and Lemarchand, 2018). Calculation of $\delta^{11}B_{sw}$ for each sample yielded similar estimates for IRC (mean +5.5‰, range +4.4 to +6.6‰) and CC (mean +5.5‰, range +5.3 to +5.9‰). Modern marine shales on continental shelves exhibit relatively low bulk $\delta^{11}B$ (median = –4.4‰, range = –6.6 to –1.8‰) due to the presence of large amounts of ^{11}B-depleted eolian dust (Spivack et al., 1987; Ishikawa and Nakamura, 1993), but open-ocean sediments contain a 'marine smectite' component with $\delta^{11}B$ (+4 to +10‰; Ishikawa and Nakamura, 1993) similar to the $\delta^{11}B_{sw}$ of the present study units.

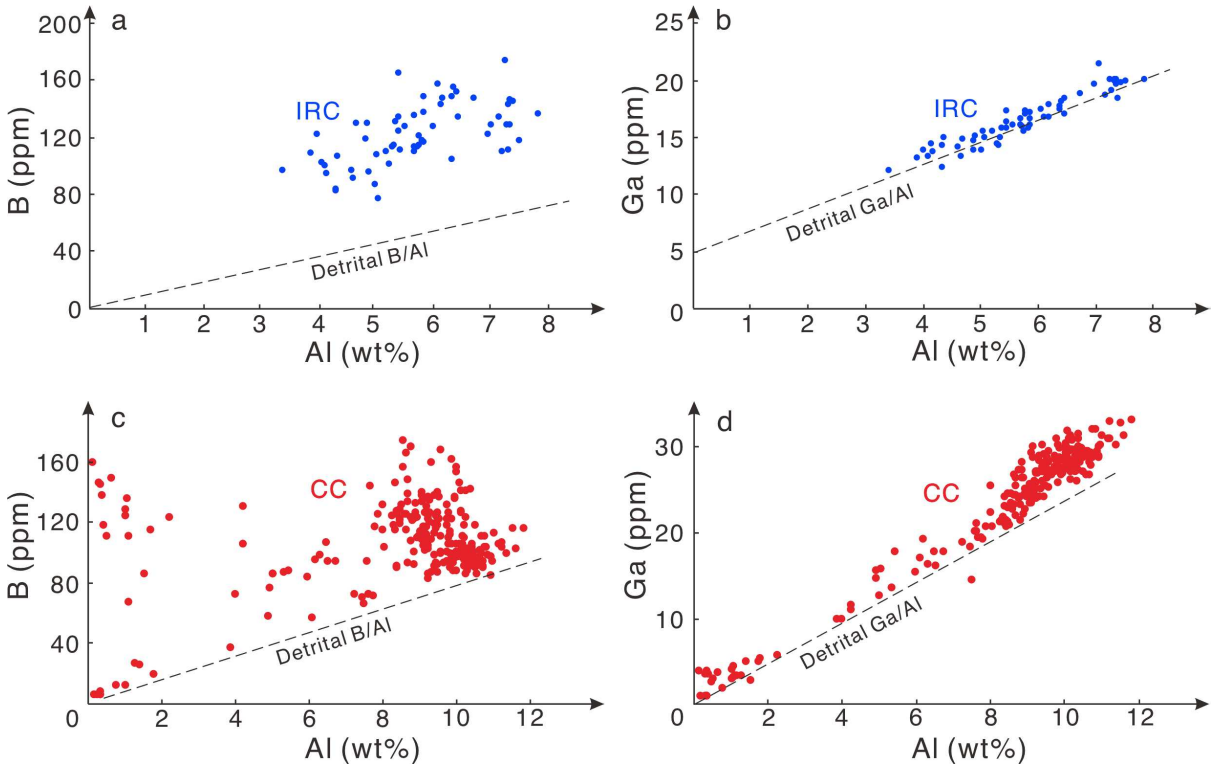

Figure S5. Crossplots of Al versus B (a,c) and Al versus Ga (b,d) for IRC (blue) and CC (red).

The dashed line in each panel represents the estimated B/Al or G/Al ratio of the detrital component. CC shows well-defined detrital ratios of 9±1 ppm/% for B/Al and 2.5 ppm/% for Ga/Al. IRC shows greater data scatter, although the detrital Ga/Al is similar to that at CC; the detrital B/Al at IRC could not be determined graphically and was assumed to be the same as at CC, which is reasonable given the similar detrital Ga/Al ratios of the two study sites.

BORON ISOTOPE SYSTEMATICS

Boron isotopes exhibit substantial variation in natural systems. During weathering, B is adsorbed onto clay-mineral surfaces (Williams et al., 2001; Ercolani et al., 2019) or becomes structurally incorporated into secondary clay minerals (Voinot, et al., 2013; Gaillardet and Lemarchand, 2018). Both processes favor uptake of ^{10}B in the solid phase by up to 30‰ (Rose et al., 2000; Noireaux et al., 2021), yielding lower $\delta^{11}B$ values for weathered clays and aeolian dust (ca. –12 ± 6‰) and higher values for riverine (+2‰ to +20‰) and meteoric waters (+1 to +26‰; Rose-Koga et al., 2006; Mao et al., 2019). Seawater B, which is mainly (>90%) sourced from rivers (Spivack et al., 1987; Gaillardet and Lemarchand, 2018), has a homogeneous $\delta^{11}B$ of +39.61 ± 0.04‰ (Ercolani et al., 2019; Mao et al., 2019) due to its long residence time (~29 Myr; Lemarchand et al., 2002).

Boron isotopic compositions are influenced by pH-controlled chemical speciation, with $B(OH)_3$ and $B(OH)_4^{-1}$ being the dominant species at low pH and high pH, respectively. In predominantly low-pH freshwater systems, B is present only as $B(OH)_3$, resulting in a uniform B-isotopic composition, whereas in seawater, both $B(OH)_3$ ($\delta^{11}B$ = +40.4 to +45.2‰) and $B(OH)_4^{-1}$ ($\delta^{11}B$ = +19.4 to +24.1‰) are present (Rose-Koga et al., 2006; Mao et al., 2019). Whereas carbonate minerals take up only the latter species, yielding marine carbonate $\delta^{11}B$ of +22.1 ± 3‰ (Hemming and Hanson, 1992), clay minerals can take up either B species depending on mineral surface charge and fluid pH, with low pH (< 7) favoring $B(OH)_4^{-1}$ uptake and high pH (> 7) favoring $B(OH)_3$ uptake (Williams et al., 2001; Kowalski and Wunder, 2018).

Modern marine carbonates faithfully record the $\delta^{11}B$ of seawater $B(OH)_4^{-1}$ (+19.4 to +24.1‰), and the $\delta^{11}B$ of carbonate samples of the present study is consistent with this B source.

The similarity of $\delta^{11}B$ values of Pennsylvanian brachiopods (+12.4 to +15.8‰; Joachimski et al., 2005) to those of modern marine brachiopods (+16.8 to +19.7‰; Lécuyer et al., 2002) implies only minor differences in the $\delta^{11}B$ of Pennsylvanian and modern seawater.

REFERENCES CITED

Berner, R. A., and Raiswell, R., 1983, Burial of organic carbon and pyrite sulfur in sediments over Phanerozoic time: a new theory: Geochimica et Cosmochimica Acta, v. 47, p. 855-862, https://doi.org/10.1016/0016-7037(83)90151-5

Ercolani, C., Lemarchand, D., and Dosseto, A., 2019, Insights on catchment-wide weathering regimes from boron isotopes in riverine material: Geochimica et Cosmochimica Acta, v. 261, p. 35-55, https://doi.org/10.1016/j.gca.2019.07.002

Gaillardet, J., and Lemarchand, D., 2018, Boron in the weathering environment, *in* Marschall, H., and Foster, G. (eds.), Boron Isotopes. Advances in Isotope Geochemistry, Springer, Cham, pp. 163-188. https://doi.org/10.1007/978-3-319-64666-4_7

Hemming, N. G., and Hanson, G. N., 1992, Boron isotopic composition and concentration in modern marine carbonates: Geochimica et Cosmochimica Acta, v. 56, p. 537-543, https://doi.org/10.1016/0016-7037(92)90151-8

Ishikawa, T., and Nakamura, E., 1993, Boron isotope systematics of marine sediments: Earth and Planetary Science Letters, v. 117, p. 567-580, https://doi.org/10.1016/0012821X(93)90103-G

Joachimski, M. M., Simon, L., Van Geldern, R., and Lécuyer, C., 2005, Boron isotope geochemistry of Paleozoic brachiopod calcite: implications for a secular change in the boron isotope geochemistry of seawater over the Phanerozoic: Geochimica et Cosmochimica Acta, v. 69, p. 4035-4044, https://doi.org/10.1016/j.gca.2004.11.017

Kowalski, P. M., and Wunder, B., 2018, Boron isotope fractionation among vapor–liquids–solids–melts: Experiments and atomistic modeling. In: Marschall, H., and Foster, G. (Eds.) Boron Isotopes: Advances in Isotope Geochemistry. Springer, Cham. https://doi.org/10.1007/978-3-319-64666-4_3

Lécuyer, C., Grandjean, P., Reynard, B., Albarède, F., and Telouk, P., 2002, $^{11}B/^{10}B$ analysis of geological materials by ICP–MS Plasma 54: application to the boron fractionation between brachiopod calcite and seawater: Chemical Geology, v. 186, p. 45-55, https://doi.org/10.1016/S0009-2541(01)00425-9

Lemarchand, D., Gaillardet, J., Lewin, E. and Allègre, C. J., 2002, Boron isotope systematics in large rivers: implications for the marine boron budget and paleo-pH reconstruction over the Cenozoic: Chemical Geology, v. 190, p. 123–140, https://doi.org/10.1016/S00092541(02)00114-6

Lemarchand, D., Cividini, D., Turpault, M. P. and Chabaux, F., 2012, Boron isotopes in different grain size fractions: Exploring past and present water–rock interactions from two soil profiles (Strengbach, Vosges Mountains): Geochimica et Cosmochimica Acta., v. 98, p. 78–93, https://doi.org/10.1016/j.gca.2012.09.009

Mao, H. R., Liu, C. Q., and Zhao, Z. Q., 2019, Source and evolution of dissolved boron in rivers: Insights from boron isotope signatures of end-members and model of boron isotopes during weathering processes: Earth-Science Reviews, v. 190, p. 439-459, https://doi.org/10.1016/j.earscirev.2019.01.016

Noireaux, J., Sullivan, P. L., Gaillardet, J., Louvat, P., Steinhoefel, G., and Brantley, S. L., 2021, Developing boron isotopes to elucidate shale weathering in the critical zone: Chemical Geology, v. 559, 119900, https://doi.org/10.1016/j.chemgeo.2020.119900

Rose, E. F. , Chaussidon, M. , and Francelanord, C., 2000, Fractionation of boron isotopes during erosion processes: the example of himalayan rivers: Geochimica et Cosmochimica Acta, v. 64, p. 397-408, https://doi.org/10.1016/S0016-7037(99)00117-9

Rose-Koga, E. F., Sheppard, S. M. F., Chaussidon, M., and Carignan, J., 2006, Boron isotopic composition of atmospheric precipitations and liquid–vapour fractionations: Geochimica et Cosmochimica Acta, v. 70, p. 1603-1615, https://doi.org/10.1016/j.gca.2006.01.003

Spivack, A. J., Palmer, M. R., and Edmond, J. M., 1987, The sedimentary cycle of the boron isotopes: Geochimica et Cosmochimica Acta, v. 51, p. 1939-1949, https://doi.org/10.1016/0016-7037(87)90183-9

Voinot, A., Lemarchand, D., Collignon, C., Granet, M., Chabaux, F., and Turpault, M. P., 2013, Experimental dissolution vs. transformation of micas under acidic soil conditions: clues from boron isotopes: Geochimica et Cosmochimica Acta, v. 117, p. 144-160, https://doi.org/10.1016/j.gca.2013.04.012

Wei, W., and Algeo, T. J., 2020, Elemental proxies for paleosalinity analysis of ancient shales and mudrocks: Geochimica et Cosmochimica Acta, v. 287, p. 341-366, https://doi.org/10.1016/j.gca.2019.06.034

Williams, L. B., Hervig, R. L., Holloway, J. R., and Hutcheon, I., 2001, Boron isotope geochemistry during diagenesis. Part I. Experimental determination of fractionation during illitization of smectite: Geochimica et Cosmochimica Acta, v. 65, p. 1769-1782, https://doi.org/10.1016/S0016-7037(01)00557-9